THE JOURNAL OF PHYSICAL CHEMISTRY B

Article

pubs.acs.org/JPCB

Near-Interfacial Halogen Atom Exchange in Collisions of Cl_2 with 2.7 M NaBr−Glycerol

Logan P. Dempsey, Jennifer A. Faust, and Gilbert M. Nathanson*

Department of Chemistry, University of Wisconsin—Madison, 1101 University Avenue, Madison, Wisconsin 53706-1322, United States

ABSTRACT: Gas−liquid scattering experiments are used to investigate reactions of Cl_2 with a 2.7 M NaBr−glycerol solution at 291 K. Only the single and double halogen exchange products, BrCl and Br_2, are observed to desorb from solution. When Cl_2 molecules strike the surface at thermal collision energies, 76% desorb as Cl_2 before reacting, 1% react to form BrCl, and 23% react to form Br_2. Residence time measurements, modeled by mass-transfer equations for absorption, diffusion, reaction, and evaporation, were used to determine the time and depth scales for Cl_2 escape and BrCl and Br_2 production. This modeling indicates that Cl_2 molecules desorb from the interfacial region in less than 1 μs or are attacked within this time by Br^- ions and irreversibly captured as Cl_2Br^-. The products BrCl and Br_2 are created primarily within the top few monolayers of the solution and then evaporate on average 12 and 28 μs after Cl_2 initially reacts with Br^-. Notably, Br_2 is not generated from BrCl via $Cl_2Br^- \rightarrow BrCl + Cl^-$ and $BrCl + Br^- \rightarrow Br_2Cl^-$ but from the parallel reaction $Cl_2Br^- + Br^- \rightarrow Br_2Cl^- + Cl^-$ that bypasses the BrCl intermediate. Br_2 is then likely released through two pathways, $Br_2Cl^- \rightarrow Br_2 + Cl^-$ and $Br_2Cl^- + Br^- \rightarrow Br_3^- + Cl^-$, followed by $Br_3^- \leftrightarrow Br_2 + Br^-$. The experiments demonstrate that single and double halogen exchange reactions can occur rapidly and close to the surface even when the products are created by multiple sequential reactions.

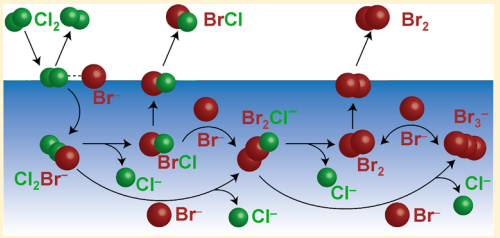

INTRODUCTION

Halide ions at gas−liquid interfaces are remarkable reagents. They may reside at or below the outermost layer of the solution,[1−7] orient solvent molecules and distort hydrogen bonds,[8−12] catalyze surface reactions,[13] and become interfacial reagents themselves.[14−18] The pioneering experiments of Hu et al. demonstrated that I^- and Br^- ions readily react with impinging Br_2 and Cl_2 molecules at the surface of water.[14] Further theoretical and experimental studies reveal the distribution of I^-, Br^-, and Cl^- ions in the interfacial region[1−4,8,10,19,20] and the diverse ways in which they react with gas-phase species. These reactions include $OH + Cl^-$,[15,21] $BrCl + I^-$,[16] and $O_3 + Br^-$ and I^-[17,22−24] at the surface of water and $Cl_2 + Br^-$ in water clusters.[25] Halide ion reactions have also been investigated at the surfaces of ice[26] and solid alkali halides.[18,27,28]

We focus here on the Cl_2/Br^- system, which is important in commerce and in the environment; the $Cl_2 + 2Br^- \rightarrow Br_2 + 2Cl^-$ reaction is used industrially to produce Br_2 by bubbling Cl_2 through brine wells rich in Br^-,[29] while the conversion of Cl_2 into BrCl and Br_2 by Br^- in snow and sea salt particles may contribute to the dramatic reduction in ozone by bromine in the Arctic.[27,30,31] The likely presence of Br^- at brine, aerosol, and snow surfaces[26,32] potentially implicates interfacial Br^- ions in the transformation of Cl_2 to BrCl and Br_2 in both industrial and atmospheric processes. In this study, we explore interfacial $Cl \rightarrow Br$ exchange by investigating reactions of Cl_2 with a 2.7 M NaBr−glycerol solution using gas−liquid scattering methods. These experiments enable us to follow the fate of Cl_2 molecules as they are captured by surface Br^- ions and then react to form the halogen exchange products BrCl and Br_2. Our objective is to learn step-by-step how the initial product of a gas−surface reaction proceeds to new products within and below the interfacial region.

Glycerol ($HOCH_2CH(OH)CH_2OH$) was chosen for these vacuum-based experiments because of its 10^{-4} mbar vapor pressure and water-like solvent properties.[33] It has a dielectric constant ε of 41 and surface tension of 63 dyn cm^{-1} at 291 K (compared with 81 and 73 dyn cm^{-1} for water) and can dissolve NaBr up to ∼4 M, close to one-half of its 9 M solubility in water. Sum frequency generation studies indicate that nearly all protic H atoms are hydrogen-bonded at the surface,[34,35] while molecular dynamics simulations predict that surface glycerol molecules expose ∼40% CH and CH_2 groups, ∼20% O, and ∼40% H from OH.[36] The surface therefore contains both hydrophobic and hydrophilic groups and no dangling hydrogen bonds, unlike that of water,[8,10,37] but for both water and glycerol, the interface is predicted to be extremely sharp and approximately one molecule thick.[36,38] The chief difference between the two solvents is the much greater viscosity of glycerol; the 2.7 M NaBr−glycerol solution used here is ∼5000 times more viscous than a 2.7 M NaBr−water solution. At this concentration, the Br^- and Na^+ ions are, on average, 7 Å apart when uniformly distributed,[39] with ∼7 glycerol OH groups per ion. This ion−ion separation is roughly equal to the Bjerrum critical distance, $e^2/(2\varepsilon kT)$,[39] suggesting

Received: August 17, 2012
Revised: September 16, 2012
Published: September 17, 2012

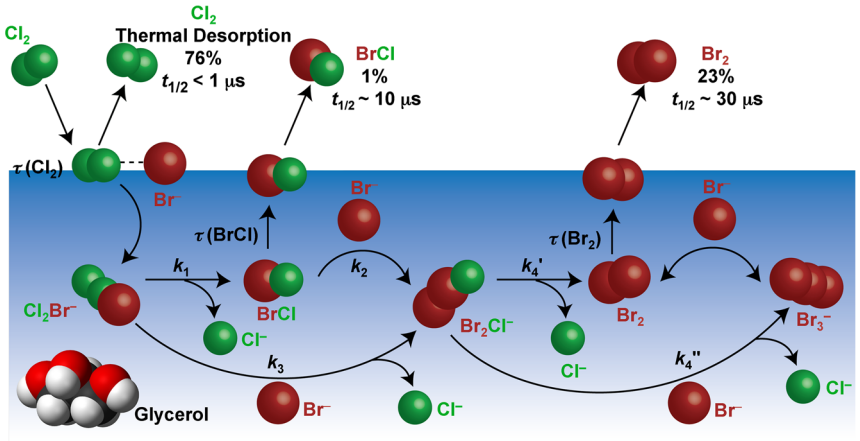

Figure 1. Scattering and reaction pathways for collisions of Cl_2 with a NaBr–glycerol solution. The half-lives $t_{1/2}$ refer to the time required for Cl_2, BrCl, and Br_2 to reach half of their steady-state desorption rates. They are determined from the rate constants k and residence times τ shown in the picture, which are extracted from the measurements and summarized later in Table 1.

that Na^+ and Br^- may often form ion pairs in the bulk and at the surface.[40]

The addition of NaBr to glycerol raises the surface tension by 3.7 dyn cm^{-1}, implying that the overall ion deficit is $\sim 6 \times 10^{13}$ cm^{-2} when integrated over the interfacial region.[41] When this deficit is restricted to the top monolayer, the resulting surface Br^- and Na^+ ion concentrations are each $\sim 7 \times 10^{13}$ cm^{-2}, and the surface glycerol concentration is 3.7×10^{14} cm^{-2}.[41] The surface OH/Br^- ratio is therefore ~10:1 when counting only exposed OH groups (for 60% OH coverage and three OH groups per molecule). Within this model, these species occupy surface areas of ~7% (Br^-), ~3% (Na^+), and ~90% (glycerol). Any preferential segregation of Br^- to the surface will increase its concentration, but this effect has not been verified in glycerol.

Figure 1 depicts the reaction pathways for Cl_2 molecules striking the surface of the NaBr–glycerol solution. Analogous reactions in bulk water have been investigated by Margerum[42,43] and Kelm[44] and their co-workers, who found that Cl_2 and Br^- react to produce Cl_2Br^- at nearly diffusion-controlled rates. This trihalide complex then decomposes into BrCl or reacts again with Br^-, ultimately producing Br_2. As described below, we find that Cl_2 molecules impinging on 2.7 M NaBr–glycerol also produce BrCl and Br_2. By coupling scattering experiments with numerical solutions of the diffusion and reaction equations, we can estimate the rate constants in Figure 1 and the average time and depth for each process. The analysis below indicates that 24% of the impinging Cl_2 react with Br^- in less than 1 μs, while BrCl and Br_2 are created from Cl_2Br^- and Br_2Cl^- at average depths of ~10 Å, followed by BrCl and Br_2 evaporation over tens of microseconds (in a ratio of Br_2/BrCl of 23:1). These short time and length scales imply that single and double Cl → Br exchange occur very close to the surface of the salty solution.

EXPERIMENTAL METHODS

The 2.7 M (2.4 *m*) NaBr–glycerol solution is prepared by adding NaBr (Aldrich, 99%) to glycerol (Aldrich, 99%) and gently heating and stirring under vacuum to dissolve the salt and remove water and air from the solution. A volume of 50 mL of solution is then added to the liquid reservoir shown in Figure 2, which depicts the apparatus used for the gas–liquid scattering experiments. A clean and continuously renewed

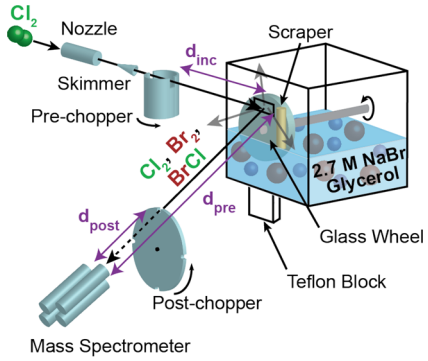

Figure 2. Scattering apparatus. The postchopper wheel (for velocity analysis) and prechopper wheel (for residence time analysis) are used alternately during an experiment. The Teflon block provides an inert surface to calibrate incident beam intensities.

liquid film is created by rotating a partially submerged 5 cm diameter glass wheel through the solution, which is maintained at 291 K.[45] The vertical film on the wheel is then skimmed to a uniform, 0.5 mm thickness by a Teflon scraper. After scraping, the wheel rotates in front of a 12×6 mm^2 rectangular hole in the reservoir, where it is exposed to a beam of Cl_2 molecules at an incident angle θ_{inc} of 45°.

Molecular beams of Cl_2 at high ($E_{inc} = 58 \pm 6$ kJ mol^{-1}) and low ($E_{inc} = 12 \pm 1$ kJ mol^{-1}) energy are created by seeding 3% Cl_2 in He and 5% Cl_2 in Ar, respectively, and expanding the gas mixture at 700 mbar through a 0.1 mm diameter pinhole nozzle. The nozzle is heated to 390 K to suppress cluster formation. Cluster distributions were gauged by directing the incident beam into the mass spectrometer and measuring the ion ratio $Cl_2^+/(Cl_2)_2^+$. The ion ratios were found to be 2100:1 for 3% Cl_2/He and 120:1 for 5% Cl_2/Ar. Argon clustering with Cl_2 was also investigated by measuring the ion ratio $Cl_2^+/(Cl_2Ar)^+$ in the 5% Cl_2/Ar beam, which was found to be 600:1. These large ion ratios imply negligible clustering in the incident beams. An additional experiment was performed using Br_2 at $E_{inc} \approx 150$ kJ mol^{-1}, which was created by bubbling H_2 over frozen Br_2 at 243 K.

Molecules scattering or desorbing from glycerol or Teflon are detected by a quadrupole mass spectrometer oriented at $\theta_{exit} = 45°$ to the reservoir. Their velocities are measured using the postchopper wheel, while their residence times in solution are

dx.doi.org/10.1021/jp308202k | J. Phys. Chem. B 2012, 116, 12306–12318

measured using the prechopper wheel.[46] With the postchopper wheel in position, the molecular beam continuously strikes the surface, exposing a patch of liquid to the incident beam for typically 0.12 s as the patch rotates in front of the hole in the reservoir. This exposure time may be varied from 0.047 to 0.47 s by adjusting the speed of the liquid-coated wheel. The exiting Cl_2, BrCl, or Br_2 species are then chopped into 80 μs pulses by the spinning postchopper wheel before traveling a distance d_{post} = 19.6 cm to the mass spectrometer. With the prechopper wheel in position, the incident Cl_2 beam is divided into 80 μs pulses before striking the liquid. An exposure time of 0.12 s permits 30 pulses to strike the same patch of liquid in 4.0 ms intervals. In this prechopper mode, the arrival time of the Cl_2, BrCl, or Br_2 species at the mass spectrometer is the sum of the gas-phase flight times of the molecules before and after interaction with the liquid and their residence time in the solution. These flight times occur over distances of d_{inc} = 6.0 cm and d_{pre} = 25.4 cm, respectively. The prechopper method can be used to monitor characteristic residence and reaction times of solution-phase species on the 10^{-6} to 10^{-2} s time scale, as shown later.[46,47]

RESULTS AND ANALYSIS

A search for reaction products indicates that BrCl and Br_2 desorb from the NaBr−glycerol solution upon exposure to Cl_2. No reaction products (less than 0.1%) could be detected from reaction of Cl_2 with pure glycerol. In particular, there was no evidence for HCl, HOCl, or $Cl(C_3H_7O_2)$ that might arise from reactions of Cl_2 with glycerol molecules in the pure or salty solutions. Additionally, no HBr or $Br(C_3H_7O_2)$ could be detected from reaction of the BrCl or Br_2 products with glycerol.[48] To investigate the production of BrCl and Br_2, we measured the uptake of Cl_2, the branching between BrCl and Br_2 products, and the time scales for Cl_2, BrCl, and Br_2 desorption.

Cl_2 Uptake into 2.7 M NaBr−Glycerol. The net uptake of Cl_2 into NaBr−glycerol is equal to the fraction of incoming Cl_2 molecules that disappear into solution and do not desorb during the exposure time t_{exp} of the rotating film, which can be varied from 0.047 to 0.47 s. Our measurements below indicate that only Cl_2 molecules that react irreversibly disappear over these long times. The uptake is determined by measuring the flux of Cl_2 molecules J_{hit} that strike the surface and the flux J_{return} that return to the gas phase.

$$\gamma^{Cl_2}(t_{exp}) = \frac{J_{hit} - J_{return}(t_{exp})}{J_{hit}} = \frac{\int N_{pure}(t_{arr})\,dt_{arr} - \int N_{NaBr}(t_{arr})\,dt_{arr}}{\int N_{pure}(t_{arr})\,dt_{arr}} \quad (1)$$

J_{return} consists of Cl_2 molecules that scatter directly, become trapped at the surface and then desorb, or dissolve and then desorb. The net uptake γ^{Cl_2} is the difference between the fraction of Cl_2 molecules that enter and the fraction that desorb; it starts at $\gamma = \beta \leq 1$, where β is the probability that Cl_2 enters solution as molecular Cl_2 or as Cl_2Br^- after reaction at the surface. $\gamma^{Cl_2}(t_{exp})$ will drop with increasing t_{exp} if some Cl_2 molecules desorb back into the gas phase over the chosen time interval, which is varied from 0.047 to 0.47 s.

J_{hit} and J_{return} are typically measured as Cl_2 partial pressures using the King and Wells reflectivity method,[49,50] but we were unable to record stable values because Cl_2 sticks too strongly to the chamber walls. We instead measure the fluxes by recording Cl_2 postchopper TOF spectra $N(t_{arr})$ versus arrival time t_{arr}, as justified below for low Cl_2 collision energies. The incident Cl_2 beam is first directed at the surface of pure glycerol, which does not react with Cl_2; the integral of the Cl_2 TOF signal N_{pure} is then proportional to J_{hit}. To measure J_{return}, the Cl_2 beam is then directed at the 2.7 M NaBr solution, and the TOF signal N_{NaBr} is recorded at different exposure times.[51]

The uptake measurements were performed with an incident Cl_2 beam at E_{inc} = 12 kJ mol^{-1} ($5RT_{liquid}$) and at θ_{inc} = 45°. At this low collision energy, nearly all Cl_2 molecules desorb in a Maxwell−Boltzmann (MB) distribution at the 291 K temperature of the pure or salty solution, as shown in Figure 3 at θ_{fin} = 45°, indicating that they thermally equilibrate upon collision before desorbing. This full equilibration implies that the uptake measured at E_{inc} = 12 kJ mol^{-1} and θ_{inc} = 45° should be close to the uptake under thermal collision conditions, where E_{inc} = $2RT_{liquid}$ = 5 kJ mol^{-1}. On the basis of this equilibration, we assume that the angular distributions of Cl_2 molecules exiting as pure and with salty glycerol are identical (likely cosine). In this case, the TOF signal measured at θ_{fin} = 45°, $\int N(t_{arr})\,dt_{arr}$, is proportional to the total flux J of Cl_2 molecules integrated over all exit angles, and the first equality in eq 1 involving total fluxes can be replaced by the second equality involving only measurements at θ_{fin} = 45°. This procedure has been verified previously for collisions of DCl with salty glycerol.[52]

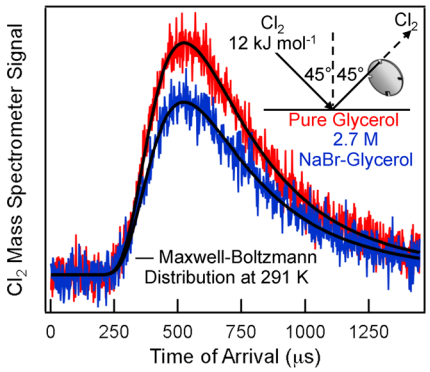

Figure 3. Postchopper time-of-flight (TOF) spectra of Cl_2 following collisions of 12 kJ mol^{-1} Cl_2 with pure glycerol (red) and 2.7 M NaBr−glycerol (blue). Solid lines (black) are MB distributions at the 291 K temperature of the solutions.

The measured value of γ^{Cl_2} is found from Figure 3, and three additional trials are found to be 0.24 ± 0.03 (90% confidence interval). The TOF spectra in Figure 3 do not change when t_{exp} is varied from 0.047 to 0.47 s, indicating that nonreacting Cl_2 molecules desorb over times shorter than 0.047 s. As shown later using Cl_2 pulsed beams, Cl_2 desorption occurs in less than 10^{-6} s, implying that 24% of the incoming Cl_2 molecules react with Br^- ions on a similar time scale.

Identification of BrCl and Br_2 Products. We next measured BrCl and Br_2 postchopper TOF spectra in order to characterize their production. Figure 4a compares the Br_2 (red) TOF spectrum with the Cl_2 (green) spectrum at E_{inc} = 12 kJ mol^{-1} ($5RT_{liq}$). Each spectrum is fit well by MB distributions (black lines) at the 291 K temperature of the solution, indicating that product Br_2 as well as nonreacting Cl_2 thermally equilibrate before exiting the solution. BrCl could only be detected by substituting a Cl_2 beam at E_{inc} = 58 kJ mol^{-1} ($24RT_{liq}$), which has ~10 times greater flux than the 12 kJ

dx.doi.org/10.1021/jp308202k | J. Phys. Chem. B 2012, 116, 12306−12318

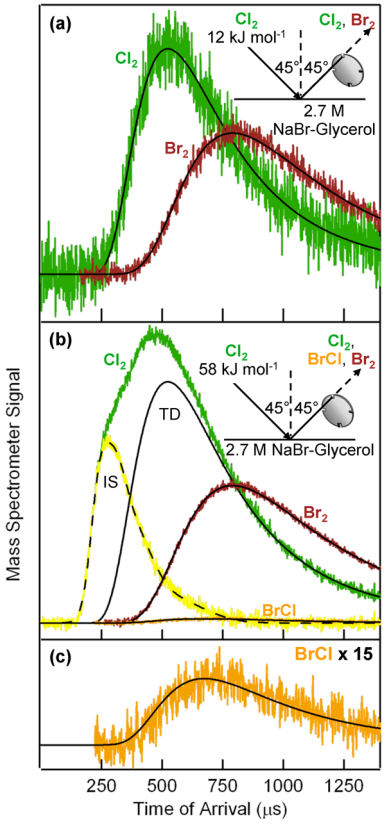

Figure 4. (a) Postchopper spectra of Cl_2 (green) and Br_2 (red) following collisions of 12 kJ mol^{-1} Cl_2 with 2.7 M NaBr−glycerol. (b) Postchopper spectra of Cl_2 (green), Br_2 (red), and BrCl (orange) following collisions of 58 kJ mol^{-1} Cl_2 with 2.7 M NaBr−glycerol. The IS and TD components of the Cl_2 spectrum are shown in yellow and black. (c) The BrCl spectrum shown in (b) magnified by 15. The solid lines in each panel are MB distributions at the 291 K temperature of the solution.

mol^{-1} beam. At this higher incident energy, Cl_2 undergoes both direct inelastic scattering (IS, dashed line) and thermal desorption (TD, solid line), as shown in panel b along with Br_2 (red) and BrCl (orange). The BrCl signal is magnified by 15-fold in panel c, whose good MB fit indicates that this single halogen exchange product also thermally equilibrates before desorbing.

The weak BrCl signal in Figure 4 indicates that nearly all Cl_2 molecules that react with Br^- ultimately produce Br_2. Importantly, the ratios of Br_2 to Cl_2 signals are nearly equal at 12 kJ mol^{-1} (0.31 ± 0.04) and 58 kJ mol^{-1} (0.028 ± 0.04) when only the Cl_2 TD component is taken into account at 58 kJ mol^{-1}. This equality implies that only thermally equilibrated Cl_2 molecules generate Br_2 and BrCl, while those Cl_2 molecules that recoil directly spend too little time at the surface to react with Br^-.

BrCl and Br_2 Branching Fractions. The Cl_2, BrCl, and Br_2 signals recorded in Figure 4 can be converted into relative production rates. This analysis requires knowledge of the ion transmission efficiency of the mass spectrometer and the relative partial ionization cross sections upon electron impact in the mass spectrometer of Cl_2, Br_2, and BrCl into Cl_2^+, Br_2^+, and $BrCl^+$. A detailed analysis in Appendix I leads to relative product fluxes of gaseous Cl_2, BrCl, and Br_2 of 1, 0.014 ± 0.003, and 0.31 ± 0.04, respectively (90% confidence intervals for six measurements). The product branching fractions for BrCl and Br_2 are therefore 4.4 ± 0.6 and 95.6 ± 0.6%. Of the Cl_2 molecules that thermalize on the surface of the salty solution, 76 ± 3% desorb before reaction, 1.0 ± 0.2% desorb as BrCl, and the remaining 23 ± 3% desorb as Br_2. The time scales for these processes are investigated below in order to explore when and where in the salty solution Cl_2 molecules react and BrCl and Br_2 are created.

Residence Times for Cl_2, BrCl, and Br_2. The bulk-phase residence and reaction times of each species in solution were measured by directing 80 μs pulses of Cl_2 at the solution using the prechopper wheel shown in Figure 2 and monitoring the time delay before Cl_2, BrCl, and Br_2 desorb. This analysis yields the rate constants k_1−k_4 and residence times τ for Cl_2, BrCl, and Br_2, pictured in Figure 1. We used high-energy, 58 kJ mol^{-1} Cl_2 molecules in these experiments for two reasons, (1) Cl_2 IS occurs on a picosecond time scale, providing a start time for measuring microsecond bulk-phase residence times, and (2) the higher flux of this beam is necessary in order to detect weak BrCl desorption. In the prechopper mode in Figure 2, the arrival time at the mass spectrometer is the sum of the gas-phase flight times of the molecules before and after interaction with the liquid and the time that they spend in solution.[46,47] The effect of this solution-phase residence time on the prechopper spectrum N_{sim} is simulated by convoluting the desorption probability $p_{des}(t)$ of Cl_2, BrCl, or Br_2 with a MB distribution N_{MB} of arrival times

$$N_{sim}(t_{arr}) = \int_0^{t_{arr}} p_{des}(t) N_{MB}(t_{arr} - t)\, dt \quad (2)$$

where $p_{des}(t) = J_{des}(t)/J_{in}(Cl_2)$ is the probability that Cl_2, BrCl, or Br_2 desorbs at time t and J_{des} is the flux of the evaporating molecule. As shown below, p_{des} can be used to determine the average time for destruction of Cl_2 and production of BrCl and Br_2. It is important to note that the diffusion−reaction equations used to calculate p_{des} in Appendix II treat the gas−liquid boundary as an infinitely sharp separation between bulk gas and bulk liquid. We then associate short reaction times with shallow depths that may be as thin as one glycerol molecule.

Submicrosecond Cl_2 Residence Time. The desorption probabilities are obtained by comparing the shapes and relative intensities of the pre- and postchopper TOF spectra, as shown in Figure 5 for Cl_2. The postchopper spectrum is displayed on the prechopper time axis by scaling the postchopper arrival times by the distance ratio d_{pre}/d_{post} in Figure 2 and adjusting the arrival times and signal levels until the post- and prechopper IS components coincide.[46] We scale the IS components to each other because impulsive scattering occurs on the picosecond time scale and will not create a measurable time delay in the prechopper spectrum. These same shifting and scaling factors are also used to compare the BrCl and Br_2 pre- and postchopper spectra. Residence times greater than 10^{-6} s will broaden and shift the MB arrival time distribution to longer arrival times because a fraction of the molecules will diffuse deeply and desorb at later times. In contrast, the postchopper spectrum corresponds to zero residence time in solution because the Cl_2 molecules strike the liquid continuously and the product signals are measured at steady state. The postchopper arrival times therefore only provide information about the velocities of the exiting molecules.

Figure 5c shows that the Cl_2 postchopper (blue) and prechopper (orange) spectra are identical in both the IS (yellow) and TD (black line) channels, implying that the Cl_2 residence time in 2.7 M NaBr−glycerol is too short to measure

dx.doi.org/10.1021/jp308202k | J. Phys. Chem. B 2012, 116, 12306−12318

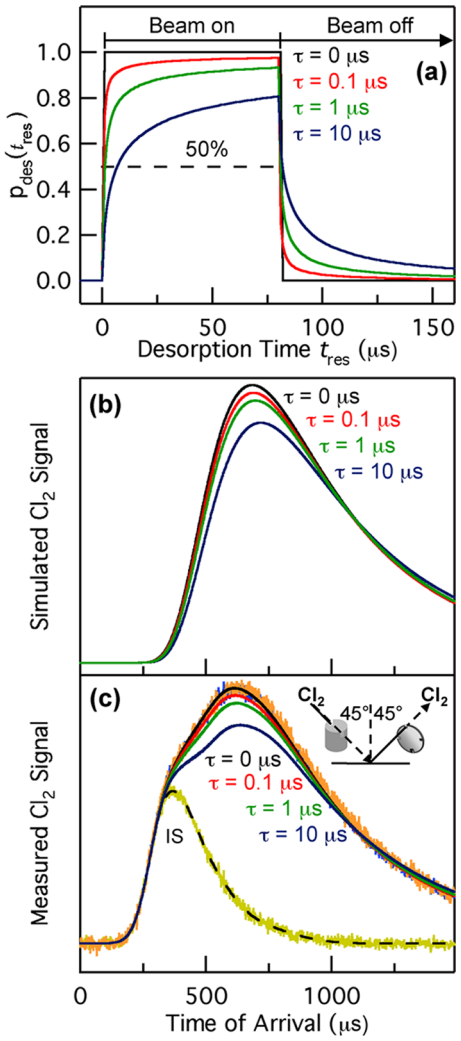

Figure 5. (a) Desorption probability $p_{des}(t_{res})$ for τ = 0 (black), 0.1 (red), 1 (green), and 10 μs (blue) for an 80 μs gas pulse. (b) Simulated thermal desorption components of Cl_2 prechopper spectra generated by convoluting p_{des} with a Cl_2 MB distribution at 291 K (see eq 2). (c) Prechopper (orange) and postchopper (blue) spectra of Cl_2 for collisions at E_{inc} = 58 kJ mol^{-1}. The IS pathway is in yellow. Solid lines are the simulated Cl_2 spectra for τ = 0 (black), 0.1 (red), 1 (green), and 10 μs (blue) residence times generated by summing the Cl_2 IS component with simulated TD components in (b).

in either direct scattering or upon thermal desorption. Similarly, identical pre- and postchopper spectra were recorded for Cl_2 scattering from pure glycerol. The minimum measurable residence time for nonreacting Cl_2 can be simulated by solving the diffusion equation for absorption and desorption in both the beam-on (0−80 μs) and beam-off (81−4000 μs) regions, as shown in panels a and b of Figure 5 and described in Appendix II. In the beam-on region, the desorption probability $p_{des}(t)$ can be analytically expressed as $1 - e^{(t/\tau)}\,\mathrm{erfc}(t/\tau)^{1/2}$, where τ is a characteristic residence time at which the outgoing gas flux reaches 57% of the steady incoming flux.[53]

Figure 5a displays $p_{des}(t)$ for τ = 0, 0.1, 1, and 10 μs, which broaden with increasing τ in both the beam-on and beam off-regions. The simulated TOF spectra obtained from eq 2 are shown in panel b. They reveal that longer solvation times spread and shift the simulated signal over longer arrival times even when τ is much smaller than the 80 μs pulse width, as shown in Figure 5b. This effect arises because a small fraction of molecules diffuse deeply and then desorb over long times; even for τ = 1 μs, p_{des} reaches only 93% of its asymptotic value by the end of the 80 μs pulse. The fits in panel c indicate that the characteristic residence time for Cl_2 is less than 1 μs, which corresponds to a characteristic diffusion depth smaller than $0.6(D\tau)^{1/2}$ = 3 Å for a transit time of $\tau/2$ and a Cl_2 diffusion constant D of 3 × 10^{-9} cm^2 s^{-1} (see Appendix II). This depth is roughly equal to the ∼5 Å thickness of one glycerol molecule. The identical pre- and postchopper spectra and simulations therefore imply that thermally accommodated Cl_2 molecules either desorb rapidly from the interfacial region or react immediately within this region; there is no indication that Cl_2 molecules diffuse deeply and return to the surface to desorb. As shown in Appendix II, the identical pre- and postchopper spectra may equivalently be fit with a bulk-phase Cl_2 reaction rate exceeding 10^6 s^{-1}, which approaches the diffusion-controlled limit.[54] The identical pre- and postchopper spectra, and the submicrosecond residence and reaction times that they imply, are our most direct evidence that the reaction of Cl_2 with Br^- occurs in the interfacial region, generating Cl_2Br^- as the species most likely to enter solution, as first stated by Hu et al. for collisions of Cl_2 with 0.5 M NaBr−H_2O.[14]

Ten Microsecond Br_2 Residence Time. In contrast to rapid Cl_2 desorption, Br_2 molecules dissolve in 2.7 M NaBr−glycerol for measurable times. The characteristic Br_2 lifetime in solution is best measured by substituting Br_2 for Cl_2 in the incident beam and directly recording the Br_2 pre- and postchopper spectra, as shown in Figure 6. In this way, the Br_2 residence time can be isolated from the reaction time required to convert Cl_2 into Br_2. The best fit to the Br_2 prechopper spectrum in Figure 6b is obtained using the p_{des} functions in panel a, which

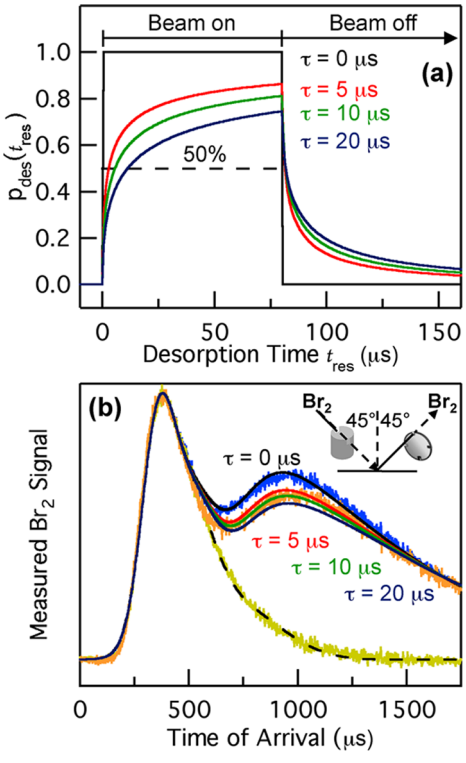

Figure 6. (a) Desorption probability $p_{des}(t_{res})$ for τ = 0 (black), 5 (green), 10 (red), and 20 μs (blue) for an 80 μs gas pulse. (c) Prechopper (orange) and postchopper (blue) spectra of Br_2 for scattering from 2.7 M NaBr−glycerol. See the caption to Figure 5.

dx.doi.org/10.1021/jp308202k | J. Phys. Chem. B 2012, 116, 12306−12318

yield $\tau = 10 \pm 5$ μs. Over this time, Br_2 diffuses a distance of ~10 Å, assuming that $D \approx 3 \times 10^{-9}$ cm^2 s^{-1}.

The characteristic residence time τ can be expressed as $\tau = D(4HRT/\beta\langle v\rangle)^2$, where H is the combined solubility in M atm^{-1} of Br_2 and Br_3^-, β is the probability that Br_2 enters the solution as Br_2 or as Br_3^- after reacting with Br^- at the surface, and $\langle v\rangle = (8RT/\pi m_{Br_2})^{1/2}$.[42,53,55,56] The time τ therefore increases with solubility and diffusivity and decreases as fewer Br_2 or Br_3^- enter solution. This equation provides an upper limit to H of 1×10^4 M atm^{-1} because β must be less than or equal to 1. In separate experiments, the pre- and postchopper spectra (not shown) were measured for Br_2 collisions with pure glycerol and found to be nearly identical, yielding a bulk-phase Br_2 solvation time shorter than 1 μs. The characteristic 10 μs residence time for Br_2 in 2.7 M NaBr–glycerol is therefore driven by its reversible reaction with Br^- to form Br_3^-, just as in water (where the Br_2 solubility increases from 1 to 15 M atm^{-1} in 0 to 2.7 M NaBr-H_2O).[57]

The 10 μs Br_2 and <1 μs Cl_2 residence times and 24% Cl_2 uptake are used below, along with the BrCl and Br_2 pre- and postchopper spectra, to determine the rates of Br_2 and BrCl production from the reaction between Cl_2 and Br^-. We also use them to estimate the BrCl residence time, which was not independently measured.

Kinetics of BrCl and Br_2 Production from Cl_2. To model the creation and desorption of BrCl and Br_2 from Cl_2, we must take into account the bulk-phase kinetics of four halogen reactions, as depicted in Figure 1. The diffusion and reaction equations are described in Appendix II. On the basis of the identical pre- and postchopper spectra in Figure 5c, we assume that Cl_2 reacts immediately near the surface to produce Cl_2Br^-. This species then dissolves and dissociates into BrCl with rate constant k_1 or reacts with Br^- to form Br_2Cl^- + Cl^- with rate constant k_3. BrCl can also react to form Br_2Cl^- with rate constant k_2. Finally, Br_2Cl^- is converted into Br_2 either by dissociation into Br_2 + Cl^- (with rate constant k_4') or by Br^- attack to form Br_3^-(with rate constant k_4''), which then reversibly dissociates into Br_2. These two parallel processes are modeled with a single, empirical rate constant k_4.

The reverse reaction rates are set equal to zero for BrCl + Cl^- (k_{-1}), Br_2Cl^- + Cl^- (k_{-3}), and Br_2 + Cl^- (k_{-4}') because the 2.7 M concentration of Br^- greatly exceeds the millimolar concentration of Cl^- from Cl_2[58] and because the rate constants are larger for Br^- than for Cl^- reactions in water.[59] The reaction BrCl + Br^- → Br_2Cl^- is also not considered to be reversible because Br_2Cl^- in water likely falls apart more readily to Br_2 + Cl^- (k_4') than to BrCl + Br^- (k_{-2}).[43,44,60] In addition to these condensed-phase reactions, BrCl and Br_2 molecules at the gas–liquid boundary may also desorb. The desorption constants may be expressed in the form $k_{des} = (D/\tau)^{1/2}$, where τ is the characteristic residence time referred to previously (see Appendix II).[53]

The pre- and postchopper spectra for BrCl and Br_2 are shown in Figure 7. Panel b reveals that the BrCl prechopper signal (gray) is weaker than the postchopper signal (blue), implying that the production and desorption of BrCl occur on the microsecond time scale, in contrast to the submicrosecond desorption of Cl_2. The Br_2 prechopper spectrum is even shallower and more shifted than the BrCl spectrum. The two prechopper spectra were fit by trial and error selection of the parameters k_1, k_2, k_3, k_4, and τ_{BrCl} and by setting $\tau_{Br_2} = 10$ μs and $\tau_{Cl_2} < 1$ μs, as determined above. Despite an extensive search,

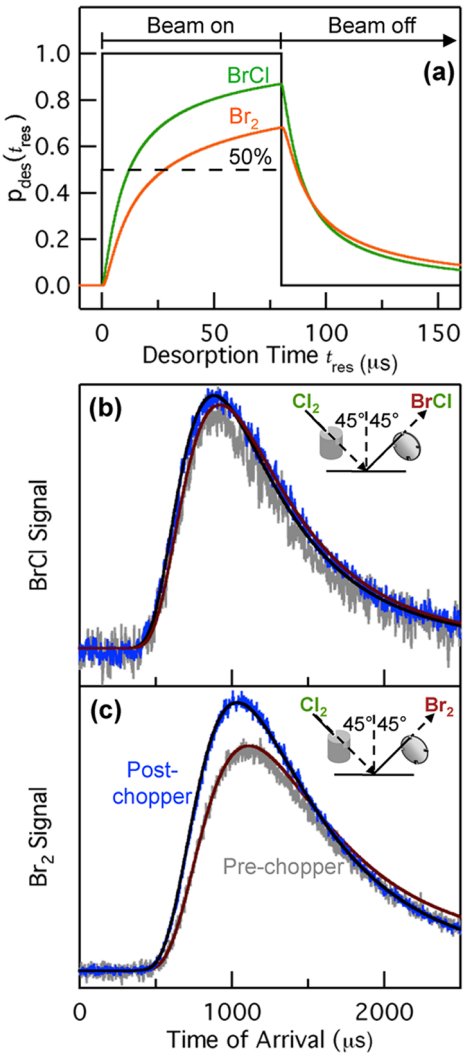

Figure 7. (a) Relative desorption flux $p_{des}(t_{res})$ for BrCl (green) and Br_2 (orange) generated by diffusion–reaction equations described in Appendix II. The black square pulse represents the instantaneous formation and desorption of products. (b,c) Prechopper (gray) and postchopper (blue) spectra of BrCl and Br_2 desorbing from 2.7 M NaBr–glycerol. The black curves through the postchopper spectra are MB distributions at 291 K. The red curves through the prechopper spectra are obtained by convoluting $p_{des}(t_{res})$ with MB distributions (eq 2).

we were unable to find one set of parameters that precisely simulates the relative intensities and shapes of the BrCl and Br_2 pre- and postchopper spectra and the 4:96 BrCl/Br_2 branching ratio. Our best attempt is shown in panels b and c using the p_{des} functions in panel a, which were obtained using the rate constants in Figure 8. The simulated prechopper spectra are slightly too broad and too high; we are unable to improve the fits because variations in rate constants that lower the simulated prechopper signal also broaden it. It might be possible to achieve better fits by using different diffusion coefficients for each species (see Appendix II) or by employing diffusion and rate constants that vary with depth. More fundamentally, some BrCl and Br_2 molecules created near the surface may desorb with a time dependence that cannot be modeled by bulk-phase diffusion and reaction.

Rate Constants in Table 1: Uncertainties and Comparison with Water. The rate constants for reaction of Cl_2 with 2.7 M

dx.doi.org/10.1021/jp308202k | J. Phys. Chem. B 2012, 116, 12306–12318

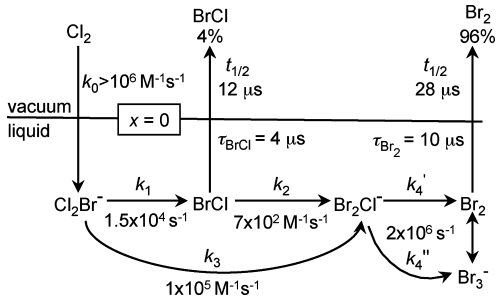

Figure 8. The diffusion–reaction–desorption model used to generate $p_{des}(t_{res})$ for BrCl and Br_2 shown in Figure 7. The best-fit values for k_1, k_2, k_3, k_4, and τ_{BrCl} are shown. τ_{Br_2} was measured separately to be 10 μs, and k_0 is determined in Appendix II. $k_4 = 2 \times 10^6$ s^{-1} represents the overall rate constant for conversion of Br_2Cl^- into Br_2 by (k_4') $Br_2Cl^- \rightarrow Br_2 + Cl^-$ and by (k_4'') $Br_2Cl^- + Br^- \rightarrow Br_3^- + Cl^-$ and $Br_3^- \rightarrow Br_2 + Br^-$.

NaBr–glycerol inferred from the diffusion–reaction model are compared in Table 1 with known rate constants in water at a

Table 1. Rate Constants for Reactions of Cl_2 with Br^- in Glycerol and in Water in Figure 8

	glycerol[a]	water[a]
Cl_2 entry probability	0.24	~0.23[b]
k_0 (M^{-1} s^{-1})	>10^6[c]	7.7[e], 6.0[c] × 10^9
k_1 (s^{-1})	1.5 × 10^4	1.7 × 10^5[d]
k_2 (M^{-1} s^{-1})	7 × 10^2	>10^8[e]
k_3 (M^{-1} s^{-1})	1 × 10^5	3.0 × 10^8[e]
k_4 (s^{-1})	2 × 10^6	unknown
τ_{BrCl} (μs)[f]	4	>1 × 10^{-4}
τ_{Br_2} (μs)[f]	10	>2 × 10^{-4}
H_{BrCl} (M atm^{-1})[g]	<9 × 10^3	0.9[f]
H_{Br_2} (M atm^{-1})[g]	<1 × 10^4	0.8[f]
D (cm^2 s^{-1})[h]	3 × 10^{-9}	1.5 × 10^{-5}

[a]Composition: 2.7 M NaBr in glycerol and 1.0 M Cl^- and trace Br^- in water. Glycerol values are measured here, and water values are from the literature. [b]Estimated for 2.7 M NaBr in water from ref 62. [c]See Appendix II for an estimate. [d]Reference 44. [e]Reference 43. [f]Reference 61. [g]τ and H are the characteristic residence time and gas–liquid solubility and are related through $\tau = D(4HRT/\beta\bar{v})^2$ (see text). The inequalities are obtained by setting the BrCl or Br_2 entry probability β to be less than one. [h]References 14 and 76. The diffusion constants D were assumed to be the same for all species (Cl_2, BrCl, Br_2, Cl_2Br^-, Br_2Cl^-) in the calculations.

1.0 M ionic strength.[42−44,61] Each rate constant is smaller in glycerol than that in water, but only the 2000-fold smaller k_3 tracks the 5000-fold higher viscosity of the salty glycerol solution. In contrast, k_1 and k_2 are 10^1 and 10^5 times smaller than the water values; these choices are required to fit the prechopper spectra and the 4:96 BrCl/Br_2 steady-state branching ratio and may reflect different stabilities of the ion and neutral species in glycerol and in water. We find that 3-fold increases or decreases in k_1, k_3, or τ_{BrCl} (with compensating adjustments in the other constants) noticeably worsen the prechopper fits, while k_2 can be made smaller but not larger and k_4 can be made larger but not smaller without worsening the fits. In all cases, our efforts to fit the data converged to produce desorption probabilities that have shapes and intensities similar to the curves for BrCl and Br_2 in Figure 7a.

Perhaps the most important implication of Table 1 is that the ratio $k_3[Br^-]/k_1 \approx 20$ is large and cannot be made much smaller without significant mismatches in the prechopper fits. The best-fit rate constants predict that, at steady state, over 99% of the Br_2 molecules are produced directly from $Cl_2Br^- + Br^- \rightarrow Br_2Cl^- + Cl^-$ (reaction k_3), bypassing production of BrCl (reaction k_1). Thus, nearly all of the doubly exchanged Br_2 molecules are created in parallel with BrCl and not by sequential exchange $Cl_2Br^- \rightarrow BrCl + Cl^-$ and $BrCl + Br^- \rightarrow Br_2Cl^-$ (reactions k_1 and k_2). This same Br_2 production mechanism is predicted by the rate constants in water, where over 99.9% of the Br_2 molecules are generated by reaction k_3 at steady state. We note that the Cl_2 uptake of 0.24 and 4% BrCl and 96% Br_2 branching fractions measured here mimic trends found previously by Huff and Abbatt for collisions of Cl_2 with bromide-covered ice at 233 K, where the Cl_2 reaction probability was found to be 10% and the branching fractions were found to be 1–2% BrCl and 98–99% Br_2.[26] It is intriguing to speculate that Br_2 might be produced in parallel with BrCl rather than from it on cold ice surfaces as well.

BrCl and Br_2 Appearance Times. The best-fit rate constants and residence times in Figure 8 determine the overall times for converting gaseous Cl_2 into gaseous BrCl and Br_2. We set these time intervals equal to the time required for p_{des} to reach 0.5, which corresponds to BrCl and Br_2 desorption fluxes equal to 50% of their steady-state fluxes. Figure 7a indicates that these half-lives are $t_{1/2}$ = 12 μs for BrCl and 28 μs for Br_2, which imply overall diffusion depths of $0.6(Dt_{1/2})^{1/2} \approx 10$ Å for BrCl and 17 Å for Br_2 (Appendix II). The longer half-life for desorbing Br_2 arises mostly from its longer bulk-phase residence time, which is enforced by its rapid equilibrium with Br_3^-.

The concentration profiles for Cl_2Br^-, BrCl, Br_2Cl^-, and Br_2, graphed in Figure 9 and calculated in Appendix II, can be used to gauge where BrCl is created from Cl_2Br^- and where Br_2 is created from Br_2Cl^-. As shown in panel a, the average diffusion depths are only ~10 Å for both Cl_2Br^- and Br_2Cl^-, implying that BrCl and Br_2 are each produced within a few monolayers of the surface. These profiles also reveal that desorbing BrCl molecules account for ~1/3 of the total BrCl molecules produced within solution over its 12 μs half-life, while the other 2/3 are still in solution or have reacted to form Br_2Cl^-.

DISCUSSION: Br^- IONS AS INTERFACIAL AND NEAR-INTERFACIAL REAGENTS

As shown in Figure 8 and Table 1, Br^- ions in a 2.7 M NaBr–glycerol solution readily react with Cl_2 molecules at the liquid–vacuum interface, converting 24% of the impinging Cl_2 into desorbing BrCl (1%) and Br_2 (23%) over tens of microseconds. The identical pre- and postchopper Cl_2 spectra in Figure 5 demonstrate that the initial reaction, $Cl_2 + Br^- \rightarrow Cl_2Br^-$, occurs in less than 1 μs, which implies bulk-phase diffusion depths shorter than one glycerol molecule. This picture is in accord with reactions between Cl_2 and Br^- at the surface of water inferred by Hu et al. from the bulk-phase Br^- concentration dependence.[14] Their models predict an overall reaction probability of 0.23 for 2.7 M NaBr–water, close to our measured value of 0.24 ± 0.03 for Cl_2 in glycerol.[62] For both solvents, three times as many Cl_2 molecules desorb back into the gas phase as react with Br^- ions. As discussed below, it may be possible to understand this incomplete capture from the short surface residence time of Cl_2.

dx.doi.org/10.1021/jp308202k | J. Phys. Chem. B 2012, 116, 12306–12318

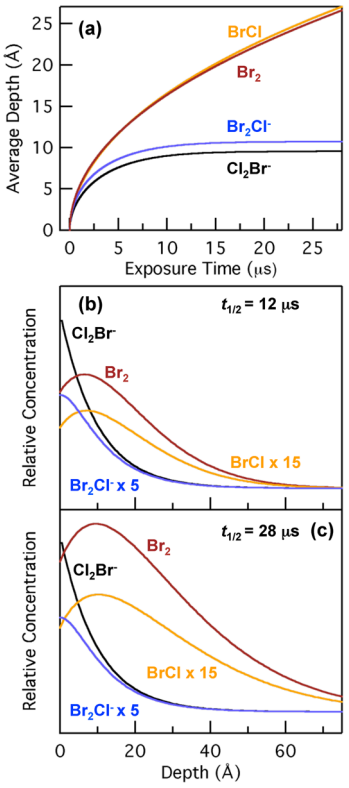

Figure 9. (a) Average diffusion depths of Cl_2Br^- (black), BrCl (orange), Br_2Cl^- (blue), and Br_2 (red) versus gas exposure time. (b,c) The concentration profiles as a function of depth at (b) $t_{1/2}$ = 12 μs for BrCl and (c) $t_{1/2}$ = 28 μs for Br_2.

Cl_2 capture likely begins when the incoming molecule is momentarily trapped at the surface by bonding to H and O atoms of the glycerol OH groups and by direct attraction to surface Br^- ions. We emphasize that the submicrosecond Cl_2 reaction time does not imply direct reactions between gas-phase Cl_2 molecules and surface Br^- ions;[63] as shown above, only thermally equilibrated Cl_2 molecules react with Br^-, most likely after the Cl_2 molecule is at least partially bonded to surface OH groups (which outnumber surface Br^- ions by approximately 10:1). This bonding strength may be considerable; ab initio calculations of Cl_2–water clusters predict binding energies that vary from 13 kJ mol^{-1} for a single H_2O–Cl_2 bond up to 40 kJ mol^{-1} for HOH–Cl_2–OH_2 bonds in a six-membered ring.[64]

The predicted 13–40 kJ mol^{-1} binding energies encompass the experimental value extracted from measurements of Cl_2 scattering from ice carried out by Pettersson and co-workers, which indicate that the residence times for Cl_2 on ice at 125–135 K are fit by a desorption energy of 26 kJ mol^{-1} and an Arrhenius prefactor of 10^{15} s^{-1}.[65] When broadly extrapolated to liquid water at 291 K, these factors predict a Cl_2 surface residence time of ~50 ps.[66] Even this short time may be sufficient to bring about reaction between Cl_2 and Br^- ions, which are separated on average by 12 Å at the surface of the 2.7 M NaBr solution. Analogous events have been analyzed theoretically by Roeselová et al., who simulated collisions of OH with the surface of a 1.2 M NaI–water solution.[67] The ~8 × 10^{13} cm^{-2} I^- surface concentration in this simulation is coincidentally similar to the 6 × 10^{13} cm^{-2} Br^- value for 2.7 M NaBr–glycerol,[68] while the 53 ps average lifetime of OH on the surface of water is also similar to the extrapolated Cl_2 lifetime.[67]

The simulations predict that OH radicals make contact with approximately seven I^- ions during their surface trajectories at an average of 2 ps per contact. Cl_2 molecules moving along the surface of glycerol might collide with a similar number of Br^- ions if the Cl_2 mobility along the surface is similar to its motion along the surface of water over a 50 ps residence time. In this case, the 24% reaction probability of Cl_2 measured here and 7 average contacts between OH and surface I^- ions from the simulation suggest that roughly 1 in 30 contacts between Cl_2 and Br^- leads to the formation of a Cl_2Br^- complex.

We can infer energetic and structural aspects of this rapid surface $Cl_2 + Br^-$ reaction from ab initio calculations using the Born solvation model by Ogawa, Takahashi, and Kakuchi, who predict that the barrier for $Cl_2 + Br^- \rightarrow [ClClBr]^-$ in water is less than RT and that the reaction is exothermic by 40 kJ/mol.[69] These predictions are in accord with the near-diffusion-controlled rates for $Cl_2 + Br^-$ measured in bulk water[43,44] of ~7 × 10^9 and >10^6 M^{-1} s^{-1} measured here in glycerol,[54] as well as with Langevin collision rates for $Cl_2 + Br^-\cdot(D_2O)_{n=1-11}$ in the gas phase.[25] The linear $[ClClBr]^-$ complex is created by Br^- addition to Cl_2, as observed in an argon matrix at 15 K.[29,70] It is also possible that the more stable isomer, $[ClBrCl]^-$,[29,70−73] may be formed by Br^- insertion into the Cl–Cl bond, in analogy with gas–gas scattering studies of CsI + Cl_2 → CsCl + ICl that are consistent with a $Cs^+[ClICl]^-$ intermediate.[74]

Figure 8 indicates that the $[ClClBr]^-$ and $[ClBrCl]^-$ complexes rapidly disappear through reaction with Br^- and to a lesser extent by decomposition into BrCl and Br^-. The dominant reaction, $Cl_2Br^- + Br^- \rightarrow Br_2Cl^- + Cl^-$, may proceed by end-on attack or insertion of Br^- into $[ClClBr]^-$ or $[ClBrCl]^-$, again potentially generating two isomers, $[BrClBr]^-$ and the more stable $[BrBrCl]^-$.[70,73] The analysis in Appendix II predicts that this exchange reaction occurs on average over a depth of 2–3 monolayers. The large rate constant of $k_3 \approx 1 \times 10^5$ M^{-1} s^{-1} is ~10% of the diffusion-controlled limit in glycerol[54] and also near the diffusion limit in water.[43,44] These fast rates preclude reactions with high barriers; this criterion eliminates only $[ClBrCl]^- + Br^- \rightarrow [BrClBr]^- + Cl^-$, for which ΔH°_{rxn} is predicted to be +30 kJ mol^{-1} in water (equal to the minimum barrier height).[69] In contrast, ΔH°_{rxn} is +8 kJ mol^{-1} for $[BrClCl]^- + Br^- \rightarrow [BrClBr]^- + Cl^-$ and is exothermic for formation of the more stable $[BrBrCl]^-$ from $[BrClCl]^-$ or $[ClBrCl]^-$.[69] Attempts to distinctly identify the less stable $[BrClBr]^-$ in an argon matrix[70] or in acetonitrile[73,75] were not successful, however, suggesting that the dominant species formed near the surface is $[BrBrCl]^-$.

In the final step, Br_2 is produced from the Br_2Cl^- isomers via two pathways shown in Figure 8, $Br_2Cl^- \rightarrow Br_2 + Cl^-$ (with dissociation rate constant k_4') and $Br_2Cl^- + Br^- \rightarrow Br_3^- + Cl^-$ (with exchange rate constant k_4''), followed by reversible dissociation of Br_3^- into $Br_2 + Br^-$. The k_4' and k_4'' rate constants have not been measured in water; our fitted overall rate constant of $k_4 \approx 2 \times 10^6$ s^{-1} in glycerol approaches the diffusion limit[54] and may be too high, but it does suggest that $[BrBrCl]^-$ and $[BrClBr]^-$ live only fleetingly near the surface of the 2.7 M NaBr solution before being converted to Br_2 or Br_3^-. This tribromide complex decomposes into Br_2 and Br^- with a half-life of 10^{-8} s in water;[44] in glycerol, this decay time must be shorter than the measured characteristic Br_2 residence time of 10^{-5} s. Together, pathways k_4' and k_4'' and the short residence time of Br_2 provide a route for the rapid production of gaseous Br_2 from Br_2Cl^-.

dx.doi.org/10.1021/jp308202k | J. Phys. Chem. B 2012, 116, 12306–12318

CONCLUSIONS

A remarkable aspect of the Cl_2 + Br^- halogen exchange reactions in 2.7 M NaBr−glycerol is the rapid conversion of the initial, interfacial trihalide complex, Cl_2Br^-, into neutral and relatively insoluble species BrCl and Br_2, which then desorb in tens of microseconds from the top few layers of the solution. Of the 24% of Cl_2 collisions that lead to reaction, nearly all produce Br_2 rather than BrCl in a 23:1 ratio. The combined BrCl and Br_2 residence time and branching fraction measurements further imply that Br_2 is not produced from BrCl as an intermediate but from Cl_2Br^- + Br^- → Br_2Cl^-, followed by conversion of Br_2Cl^- into Br_2. The near-interfacial production of BrCl and Br_2, depicted in Figures 8 and 9, pertains not only to NaBr−glycerol but to NaBr−water as well. When the diffusion and reaction equations in Appendix II are applied to the water rate constants in Table 1, we find that BrCl and Br_2 are produced and evaporate ∼2000 times faster than in glycerol, in accord with the lower viscosity of water. Just as in glycerol, however, BrCl and Br_2 are mostly created within 20 Å of the surface. These calculations support conclusions of previous studies of Cl_2 with bromide-rich water and ice surfaces that Cl_2 is rapidly converted into Br_2 in or close to the interfacial region.[14,18,26]

Although Br^- is the interfacial reagent in reactions with Cl_2, the accompanying cation can dramatically alter the reactivity of the solution. Ongoing studies reveal that substituting 2.7 M NaBr with 0.03 M tetrahexylammonium bromide (THABr), a surfactant, increases the Cl_2 uptake from 24 to 78% and again produces primarily Br_2 rather than BrCl. The 0.03 M THABr solution was chosen because the interfacial Br^- concentrations are approximately equal for the two salts. This surprising threefold increase in Cl_2 reactivity implies that even tiny additions of a cationic surfactant can tease nearly all incoming Cl_2 molecules into the interfacial region and capture them long enough to react with the Br^- counterions.

APPENDIX I: BRANCHING FRACTIONS FOR GASEOUS BrCl AND Br_2

This appendix describes a procedure to determine the production rates of gaseous BrCl and Br_2 following collisions of Cl_2 molecules with NaBr−glycerol at E_{inc}= 12 kJ mol^{-1} and θ_{inc} = 45°. These production rates are proportional to the BrCl and Br_2 desorption fluxes, J_{BrCl} and J_{Br_2}, which are calculated from the TOF spectra at $\theta_{inc} = \theta_{fin}$ = 45° according to

$$J_A \propto \int n_A(t_{arr}) v_A(t_{arr})\, dt_{arr} \propto \frac{n_A}{\sqrt{m_A}} \quad (A.1)$$

for A = Cl_2, BrCl, or Br_2. In this equation, $n_A(t_{arr})$ is the number density of A at the mass spectrometer at a time of arrival t_{arr} and a velocity of $v_A = d_{post}/t_{arr}$, where d_{post} is the distance traveled by the gas-phase molecule, as shown in Figure 2. We assume that the angular distributions of the desorbing Cl_2, BrCl, and Br_2 molecules are identical (and likely cosine), such that the ratios of fluxes at θ_{fin} = 45° are the same as for the angle-integrated fluxes. The second proportionality in eq A.1 applies to molecules desorbing in a Maxwell−Boltzmann distribution, which is observed here for all species. In this equation, m_A is the mass of the gas, and n_A is the integrated number density computed from $\int n_A(t_{arr})\, dt_{arr}$. The value of n_A is directly proportional to the integrated ion signal n_{A^+} recorded in the TOF spectrum after ionization of A in the mass spectrometer.

The value of n_{Br_2}, for example, is obtained from the TOF spectrum at the $^{160}Br_2^+$ ion mass according to

$$n_{Br_2} = \frac{n^{160}{}_{Br_2^+}}{\sigma_{Br_2\rightarrow Br_2^+} T_{Br_2^+} f^{160}{}_{Br_2}} \quad (A.2)$$

where $\sigma_{Br_2\rightarrow Br_2^+}$ is the partial ionization cross section for creation of Br_2^+ from neutral Br_2, $T_{Br_2^+}$ is the efficiency of ion transmission through the mass spectrometer at the $^{160}Br_2^+$ mass, and $f^{160}{}_{Br_2}$ is the abundance of the $^{160}Br_2^+$ isotope at m/z = 160. In practice, we measure relative number densities in our experiment and therefore only need relative values for σ, T, and f to determine reaction probabilities.

We are not aware of measurements of the partial ionization cross sections of Cl_2, Br_2, and BrCl to their respective ions Cl_2^+, $BrCl^+$, and Br_2^+ at any electron energy.[77] This problem can be circumvented by measuring the combined ratio of the transmission efficiency and ionization cross section, $T\sigma$, according to

$$\frac{T_{Cl_2^+}}{T_{Br_2^+}} \frac{\sigma_{Cl_2\rightarrow Cl_2^+}}{\sigma_{Br_2\rightarrow Br_2^+}} = \frac{n_{Cl_2^+}}{n_{Br_2^+}} \frac{n_{Br_2}}{n_{Cl_2}} \frac{f_{Br_2}}{f_{Cl_2}} \quad (A.3)$$

The value of $n_{Cl_2^+}/n_{Br_2^+}$ is provided by our measurements, and the isotopic abundances are known. To determine the ratio of neutral molecule densities n_{Br_2}/n_{Cl_2}, we ignore the small production of BrCl and invoke the approximation that all Cl_2 molecules entering the solution react to form Br_2. The Cl_2 uptake is γ_{Cl_2} = 0.24 ± 0.03 ≈ $J_{Br_2}/(J_{Br_2} + J_{Cl_2})$, where J_{Cl_2} is the flux of Cl_2 that desorbs from the surface without reacting and $J_{Br_2} + J_{Cl_2}$ is 0.31 ± 0.04. Using eq A.1, we can then calculate the ratio $n_{Br_2} + n_{Cl_2}$ = 0.46 ± 0.06 and determine $(T_{Cl_2^+}\sigma_{Cl_2\rightarrow Cl_2^+})/(T_{Br_2^+}\sigma_{Br_2\rightarrow Br_2^+})$ from eq A.3 to be 0.43 ± 0.06.

Next, we refine the measurement to account for the small amount of BrCl products formed. We treat BrCl as a hybrid molecule whose combined transmission and ionization cross section is the average of the ratios measured for Cl_2 and Br_2, such that

$$\frac{T_{BrCl^+}}{T_{Br_2^+}} \frac{\sigma_{BrCl\rightarrow BrCl^+}}{\sigma_{Br_2\rightarrow Br_2^+}} = \frac{1}{2}\left(1 + \frac{T_{Cl_2^+}}{T_{Br_2^+}} \frac{\sigma_{Cl_2\rightarrow Cl_2^+}}{\sigma_{Br_2\rightarrow Br_2^+}}\right) = 0.72 \pm 0.03$$

This ratio, the measured ratio $n^{116}{}_{BrCl^+}/n^{116}{}_{Br_2^+}$, and eq A.2 yield n_{BrCl}/n_{Br_2} = 0.039 ± 0.005. The ratio of desorption fluxes J_{BrCl}/J_{Br_2} is then determined from eq A.1 to be to 0.046 ± 0.006.

Finally, the flux ratios are combined with the Cl_2 uptake to determine the BrCl and Br_2 desorption probabilities. The BrCl and Br_2 branching fractions are $J_{BrCl}/(J_{BrCl} + J_{Br_2})$ = 0.044 ± 0.006 for BrCl, and therefore, $J_{Br_2}/(J_{BrCl} + J_{Br_2})$ = 0.956 ± 0.006 for Br_2. The 0.24 ± 0.03 Cl_2 reaction probability at E_{inc} = 12 kJ mol^{-1} and θ_{inc} = 45° implies that for all Cl_2 striking the surface, 76 ± 3% desorb before reaction, 1.0 ± 0.2% desorb as BrCl, and 23 ± 3% desorb as Br_2. Values used in calculation of reaction probabilities are given in Table A.1.

dx.doi.org/10.1021/jp308202k | J. Phys. Chem. B 2012, 116, 12306−12318

Table A.1. Values for Determining Reaction Probabilities

	Cl_2^+	$BrCl^+$	Br_2^+
m/z	70	116[a]	160[b]
f	0.57	0.50	0.50
$n_{A^+}/n_{Br_2^+}$	1.08 ± 0.02	0.028 ± 0.003	1
$(\sigma_{A\rightarrow A^+}T_{A^+})/(\sigma_{Br_2\rightarrow Br_2^+}T_{160})$	0.43 ± 0.03	0.72 ± 0.03	1

[a] $^{116}BrCl$ is formed by the isotope combinations $^{79}Br^{37}Cl$ and $^{81}Br^{35}Cl$. [b] $^{160}Br_2$ is formed by the isotope combination $^{79}Br^{81}Br$.

APPENDIX II: DESORPTION PROBABILITIES FOR BrCl AND Br_2 FOLLOWING COLLISIONS OF Cl_2

This appendix describes the calculation of the desorption probabilities $p_{des}(t)$ in Figure 7 for producing gaseous BrCl and Br_2 following collisions of Cl_2 with 2.7 M NaBr−glycerol. The probability that product molecules desorb from solution at time t following Cl_2 exposure at $t = 0$ is given by $p_{des}(t) = J_{des}(t)/J_{in}(Cl_2)$, where $J_{des}(t)$ is the outgoing product flux, $J_{in}(Cl_2) = \beta J_{hit}(Cl_2)$ is the flux of Cl_2 molecules that enter the liquid, and β is the probability that Cl_2 enters solution as molecular Cl_2 or Cl_2Br^-. As shown in Figure 7, BrCl and Br_2 desorb in two regions, when the solution is exposed to a steady Cl_2 beam (beam-on region from 0 to t_{pulse}) and after the Cl_2 pulse has stopped (beam-off region from t_{pulse} up to t_{exp}). The desorption fluxes in each region are obtained by numerically solving diffusion−reaction equations for each species. These equations and flux matching conditions at the gas−liquid boundary govern absorption of the reactant and the diffusion, reaction, and desorption of intermediates and products. Our boundary conditions and reaction−diffusion equations are based on the method of Danckwerts.[53,56]

Absorption and Desorption without Reaction

We first summarize results for reversible absorption without reaction, $A_{gas} \leftrightarrows A_{liquid}$, used in Figures 5 and 6 for Cl_2 and Br_2. The liquid is assumed to be infinitely deep and initially fresh. The boundary conditions for the liquid-phase concentration $c(x,t)$ are then $c(x\rightarrow\infty,t) = 0$ and $c(x > 0, t = 0) = 0$. The fluxes in and out of the liquid are matched with the concentration gradient at the gas−liquid boundary ($x = 0$)

$$\left.\frac{-D\,\partial c(x,t)}{\partial x}\right|_{x=0} = J_{in} - J_{out}(t) \quad \text{beam-on region}$$

$$= \frac{\beta\langle v\rangle}{4(c_{gas}^* - c_{gas}(t))}$$

$$= (D/t)^{1/2}(c^* - c(x=0,t)) \equiv \gamma(t)J_{hit}$$

$$= J_{out}(t) = (D/\tau)^{1/2}c(x=0,t) \quad \text{beam-off region}$$

where $k_{des} \equiv (D/\tau)^{1/2}$ is the rate constant for transport across the gas−liquid interface, $J_{hit} = \langle v\rangle/4\ c_{gas}^*$ is the flux onto the surface, $J_{in} = \beta J_{hit}$ is the flux into the liquid, and $\gamma(t) = (J_{in} - J_{out})/J_{hit}$ is the net uptake into the liquid, which drops from β at $t = 0$ to zero at long times when the liquid is saturated with gas and $J_{out} = J_{in}$. In these expressions, c_{gas}^* is the gas-phase concentration of A in equilibrium with a uniform liquid-phase concentration c^*, which are linked by $K_{eq} = HRT = c^*/c_{gas}^*$. The quantity $c_{gas}(t)$ is the gas-phase concentration that would be in equilibrium with the liquid-phase concentration $c(x = 0,t)$ at the gas−liquid boundary, such that $c(x = 0,t)/c_{gas}(t)$ also equals HRT. The characteristic residence time τ is described in the main text and below.

The boundary conditions are then applied to the diffusion equation, $D\,\partial^2c(x,t)/\partial x^2 = \partial c(x,t)/\partial t$, to obtain the solute concentration. In the beam-on region from $t = 0$ to t_{pulse}, $c(x,t)/c^* = \mathrm{erfc}(x/(4Dt)^{1/2}) - \exp(x/(D\tau)^{1/2})\exp(t/\tau)\,\mathrm{erfc}((t/\tau)^{1/2} + x/(4Dt)^{1/2})$.[78] The desorption probability is then obtained from $p_{des}(t) = J_{out}(t)/J_{out}(t\rightarrow\infty) = J_{out}(t)/J_{in} = 1 - \gamma(t)/\beta = c(x = 0,t)/c^*$. In the beam-on region, $p_{des}(t) = 1 - \exp(t/\tau)\,\mathrm{erfc}(t/\tau)^{1/2}$,[79−81] such that $p_{des}(t_{1/2} = 0.59\tau) = 0.5$ and $p_{des}(t = \tau) = 0.57$. Thus, at exposure time $t_{1/2} = 0.59\tau$, the flux of desorbing molecules is 50% of the asymptotic desorption flux (where $J_{out}(t\rightarrow\infty) = J_{in}$) . The desorption probability does not reach 90% of J_{in} until $t = 31\tau$. Analogous quantities in the beam-off region must be solved numerically because the initial concentration, $c(x,t_{pulse})$, is not uniform.

Plots of p_{des} for Cl_2 and Br_2 are shown in Figures 5a and 6a. The average diffusion depth may be calculated from $\langle x(t)\rangle = \int xc(x,t)\,dx/\int c(x,t)\,dx$. In the beam-on region, $\langle x(t)\rangle = 0.88(Dt)^{1/2}$, such that $\langle x(\tau/2)\rangle = 0.62(D\tau)^{1/2}$ for transit times into and out of solution of $\tau/2$ each way.

Absorption and Desorption with Irreversible Reaction

The analysis above may be extended to include irreversible reaction with rate constant k_0, $A_{gas} \leftrightarrows A_{liquid} \rightarrow B_{liquid}$.[78,82,83] In this case, the diffusion equation becomes $\partial c(x,t)/\partial t = D\,\partial^2c(x,t)/\partial x^2 - k_0c(x,t)$ with the same boundary conditions above. The expression for $p_{des}(t)$ must be found numerically in the beam-off region but is analytic in the beam-on region[83,84]

$$p_{des}(t) = 1 - \frac{\beta}{(1/\tau - k_0)}[\sqrt{k_0/\tau}\ \mathrm{erf}(\sqrt{k_0 t}) + 1/\tau\ \mathrm{erfc}(\sqrt{t/\tau})\exp(t/\tau - k_0 t) - k_0]$$

At long time, $p_{des}(t)$ approaches $(1 - k_0\tau)^{1/2}/(1 - k_0\tau)$. These two expressions may be used to model the identical Cl_2 pre- and postchopper spectra with the assumption that Cl_2 reacts in the bulk solution and not at the surface. We find that $p_{des}(t)$ mimics the square pulse necessary to reproduce the prechopper spectrum when $\tau < 0.1\ \mu s$ or $k_0 > 10^6\ M^{-1}\ s^{-1}$, which approaches the diffusion-controlled reaction rate constant.[54] Thus, Cl_2 appears to react with Br^- ions in the interfacial region or as quickly as possible as it passes into the bulk phase.

Absorption and Desorption with Multiple Species and Reactions

Figure 8 depicts the reaction scheme for conversion of Cl_2 into Cl_2Br^-, BrCl, Br_2Cl^-, and Br_2, of which only the products BrCl and Br_2 can evaporate. The four diffusion−reaction equations corresponding to this scheme are

$$\frac{\partial Cl_2Br^-(x,t)}{\partial t} = D\frac{\partial^2 Cl_2Br^-(x,t)}{\partial x^2} - k_1Cl_2Br^-(x,t) - k_3Cl_2Br^-(x,t) \quad (B.1)$$

$$\frac{\partial BrCl(x,t)}{\partial t} = D\frac{\partial^2 BrCl(x,t)}{\partial x^2} + k_1Cl_2Br^-(x,t) - k_2BrCl(x,t) \quad (B.2)$$

$$\frac{\partial Br_2Cl^-(x,t)}{\partial t} = D\frac{\partial^2 Br_2Cl^-(x,t)}{\partial x^2} + k_3Cl_2Br^-(x,t) + k_2BrCl(x,t) - k_4Br_2Cl^-(x,t) \quad (B.3)$$

$$\frac{\partial Br_2(x,t)}{\partial t} = D\frac{\partial^2 Br_2(x,t)}{\partial x^2} + k_4Br_2Cl^-(x,t) \quad (B.4)$$

dx.doi.org/10.1021/jp308202k | J. Phys. Chem. B 2012, 116, 12306−12318

The scheme in Figure 8 determines the flux balancing conditions at the gas−liquid boundary ($x = 0$) for Cl_2Br^-, BrCl, Br_2Cl^-, and Br_2. In particular, Cl_2 enters the solution as Cl_2Br^- during the beam-on region, BrCl and Br_2 may desorb during both beam-on and beam-off regions, and Cl_2Br^- and Br_2Cl^- cannot desorb at any time. The four conditions are

$$\left.\frac{-D\,\partial[Cl_2Br^-]}{\partial x}\right|_{x=0} = J_{in} - J_{des} = J_{in} = \beta J_{hit}(Cl_2)$$

beam-on region (B.5a)

$$\left.\frac{-D\,\partial[Cl_2Br^-]}{\partial x}\right|_{x=0} = 0 \qquad \text{beam-off region} \tag{B.5b}$$

$$\left.\frac{-D\,\partial[BrCl]}{\partial x}\right|_{x=0} = J_{des} = -\left(\frac{D}{\tau_{BrCl}}\right)^{1/2}[BrCl(x = 0, t)] \tag{B.6}$$

$$\left.\frac{-D\,\partial[Br_2Cl^-]}{\partial x}\right|_{x=0} = 0 \tag{B.7}$$

$$\left.\frac{-D\,\partial[Br_2]}{\partial x}\right|_{x=0} = J_{des} = -\left(\frac{D}{\tau_{Br_2}}\right)^{1/2}[Br_2(x = 0, t)] \tag{B.8}$$

Equations B.1−B.4 are solved simultaneously with the boundary conditions above using backward time integration with time steps $\Delta t = 0.1$ μs and depth steps $\Delta x = 3.2$ Å for $D = 3 \times 10^{-9}$ cm^2 s^{-1} that were optimized for repeated trials. One longer simulation was performed with the best-fit parameters using a finer grid of $\Delta t = 0.001$ μs and $\Delta x = 0.3$ Å, which only altered the BrCl branching fraction from 4.3 to 4.0%, $t_{1/2}$(BrCl) from 12 to 11 μs, and $t_{1/2}(Br_2)$ from 28 to 27 μs. The desorption fluxes for BrCl and Br_2 are then obtained from eqs B.6 and B.8, and the desorption probabilities are calculated from $p_{des}(t) = J_{des}(t)/\beta J_{hit}(Cl_2)$. At long times, $J_{des}(t \rightarrow \infty)/\alpha J_{hit}(Cl_2)$ approaches 4.3% for BrCl and 95.7% for Br_2. The predicted prechopper TOF spectra are then obtained by convolving $p_{des}(t)$ with a MB arrival time distribution using eq 2 in the main text.

The parameters k_1, k_2, k_3, k_4, τ_{BrCl}, and τ_{Br_2} are adjusted until the best fit is obtained to the steady-state 4.3% BrCl and 95.7% Br_2 fluxes and the shapes and relative heights of the BrCl and Br_2 prechopper spectra in Figure 7. In the present analysis, all diffusion coefficients D are set equal, and $p_{des}(t)$ is independent of the magnitude of D. One attempt to vary the diffusion coefficients by setting $D(Cl_2Br^-) = D(Br_2Cl^-) = 1/2\ D(Cl_2) = 1/2\ D(Br_2)$ did not improve the fit. Our best fits are shown in Figure 7 and summarized in Table 1.

Lastly, Figure 9b,c shows the concentration profiles for all four species at $t_{1/2} = 12$ (BrCl) and 28 μs (Br_2), the time at which p_{des} is half of its maximum, steady-state value. These profiles may be used to calculate the average diffusion depths as a function of exposure time, shown in panel c. This panel reveals that Cl_2Br^- and Br_2Cl^- concentrations reach steady values after ~10 μs. The average depths themselves can be simply predicted from the steady-state reaction depth, $(D/(k_1 + k_3[Br^-]))^{1/2} \approx 10$ Å.

AUTHOR INFORMATION

Corresponding Author

*E-mail: gmnathan@wisc.edu.

Notes

The authors declare no competing financial interest.

ACKNOWLEDGMENTS

This material is based on work supported by the National Science Foundation under Grant No. CHE-0809681 and by a National Science Foundation Graduate Research Fellowship to J.A.F. under Grant No. DGE-0718123. We are grateful to NSF for funding this work, to Daniel Klingenberg and Arun Yethiraj for their advice in solving the mass-transfer equations in Appendix II, and to John Berry for conversations about halogen chemistry.

REFERENCES

(1) Jungwirth, P.; Tobias, D. J. *Chem. Rev.* **2006**, *106*, 1259−1281.
(2) Andersson, G.; Krebs, T.; Morgner, H. *Phys. Chem. Chem. Phys.* **2005**, *7*, 2948−2954.
(3) Ghosal, S.; Hemminger, J. C.; Bluhm, H.; Mun, B. S.; Hebenstreit, E. L. D.; Ketteler, G.; Olgetree, D. F.; Requejo, F. G.; Salmeron, M. *Science* **2005**, *307*, 563−566.
(4) Chang, T.-M.; Dang, L. X. *Chem. Rev.* **2006**, *106*, 1305−1322.
(5) Winter, B.; Faubel, M. *Chem. Rev.* **2006**, *106*, 1176−1211.
(6) Petersen, P. B.; Saykally, R. J. *Annu. Rev. Phys. Chem.* **2006**, *57*, 333−364.
(7) Gopalakrishnan, S.; Liu, D. F.; Allen, H. C.; Kuo, M.; Shultz, M. J. *Chem. Rev.* **2006**, *106*, 1155−1175.
(8) Liu, D.; Ma, G.; Levering, L. M.; Allen, H. C. *J. Phys. Chem. B* **2004**, *108*, 2252−2260.
(9) Ishiyama, T.; Morita, A. *J. Phys. Chem. C* **2007**, *111*, 721−737.
(10) Raymond, E. A.; Richmond, G. L. *J. Phys. Chem. B* **2004**, *108*, 5051−5059.
(11) Cappa, C. D.; Smith, J. D.; Wilson, K. R.; Messer, B. M.; Gilles, M. K.; Cohen, R. C.; Saykally, R. J. *J. Phys. Chem. B* **2005**, *109*, 7046−7052.
(12) Otten, D. E.; Shaffer, P. R.; Geissler, P. L.; Saykally, R. J. *Proc. Natl. Acad. Sci. U.S.A.* **2012**, *109*, 701−705.
(13) Dempsey, L. P.; Brastad, S. M.; Nathanson, G. M. *J. Phys. Chem. Lett.* **2011**, *2*, 622−627.
(14) Hu, J. H.; Shi, Q.; Davidovits, P.; Worsnop, D. R.; Zahniser, M. S.; Kolb, C. E. *J. Phys. Chem.* **1995**, *99*, 8768−8776.
(15) Knipping, E. M.; Lakin, M. J.; Foster, K. L.; Jungwirth, P.; Tobias, D. J.; Gerber, R. B.; Dabdub, D.; Finlayson-Pitts, B. J. *Science* **2000**, *288*, 301−306.
(16) Katrib, Y.; Deiber, G.; Schweitzer, F.; Mirabel, P.; George, C. *J. Aerosol Sci.* **2001**, *32*, 893−911.
(17) Clifford, D.; Donaldson, D. J. *J. Phys. Chem. A* **2007**, *111*, 9809−9814.
(18) Finlayson-Pitts, B. J. *Chem. Rev.* **2003**, *103*, 4801−4822.
(19) Dang, L. X. *J. Phys. Chem. A* **2004**, *108*, 9014−9017.
(20) Cheng, M. H.; Callahan, K. M.; Margarella, A. M.; Tobias, D. J.; Hemminger, J. C.; Bluhm, H.; Krisch, M. J. *J. Phys. Chem. C* **2012**, *116*, 4545−4555.
(21) Thomas, J. L.; Jimenez-Aranda, A.; Finlayson-Pitts, B. J.; Dabdub, D. *J. Phys. Chem. A* **2006**, *110*, 1859−1867.
(22) Enami, S.; Vecitis, C. D.; Cheng, J.; Hoffman, M. R.; Colussi, A. J. *J. Phys. Chem. A* **2007**, *111*, 13023−13027.
(23) Hunt, S. W.; Roeselová, M.; Wang, W.; Wingen, L. M.; Knipping, E. M.; Tobias, D. J.; Dabdub, D.; Finlayson-Pitts, B. J. *J. Phys. Chem. A* **2004**, *108*, 11559−11572.
(24) Enami, S.; Vecitis, C. D.; Cheng, J.; Hoffman, M. R.; Colussi, A. J. *J. Phys. Chem. A* **2007**, *111*, 8749−8752.
(25) Seeley, J. V.; Morris, R. A.; Viggiano, A. A. *J. Phys. Chem.* **1996**, *100*, 15821−15826.

(26) Huff, A. K.; Abbatt, J. P. D. *J. Phys. Chem. A* **2000**, *104*, 7284−7293.
(27) Mochida, M.; Hirokawa, J.; Akimoto, H. *Geophys. Res. Lett.* **1998**, *25*, 3927−3930.
(28) Rossi, M. J. *Chem. Rev.* **2003**, *103*, 4823−4882.
(29) Grinbaum, B.; Freiberg, M. *Bromine In Kirk-Othmer Encyclopedia of Chemical Technology*, 5th ed.; Wiley: Hoboken, 2004; Vol. *4*.
(30) Tang, T.; McConnell, J. C. *Geophys. Res. Lett.* **1996**, *231*, 2633−2636.
(31) Foster, K. L.; Plastridge, R. A.; Bottenheim, J. W.; Shepson, P. B.; Finlayson-Pitts, B. J.; Spicer, C. W. *Science* **2001**, *291*, 471−474.
(32) Ghosal, S.; Brown, M. A.; Bluhm, H.; Krisch, M. J.; Salmeron, M.; Jungwirth, P.; Hemminger, J. C. *J. Phys. Chem. A* **2008**, *112*, 12378−12384.
(33) Miner, C. S. *Glycerol*; Reinhold Publishing Corporation: New York, 1953.
(34) Baldelli, S.; Schnitzer, C.; Shultz, M. J.; Campbell, D. J. *J. Phys. Chem. B* **1997**, *101*, 4607−4612.
(35) Oh-e, M.; Yokoyama, H.; Baldelli, S. *Appl. Phys. Lett.* **2004**, *84*, 4965−4967.
(36) Benjamin, I.; Wilson, M. A.; Pohorille, A. *J. Chem. Phys.* **1994**, *100*, 6500−6507.
(37) Du, Q.; Superfine, R.; Freysz, E.; Shen, Y. R. *Phys. Rev. Lett.* **1993**, *70*, 2313.
(38) Stiopkin, I. V.; Weeraman, C.; Pieniazek, P. A.; Shalhout, F. Y.; Skinner, J. L.; Benderskii, A. V. *Nature* **2011**, *474*, 192−195.
(39) Robinson, R. A.; Stokes, R. H. *Electrolyte Solutions*, 2nd ed.; Academic Press: New York, 1959; Chapter 14, p 15.
(40) Cwiklik, L.; Andersson, G.; Dan, L. X.; Jungwirth, P. *ChemPhysChem* **2007**, *8*, 1457.
(41) Brastad, S. M.; Albert, D. R.; Huang, M.; Nathanson, G. M. *J. Phys. Chem. A* **2009**, *113*, 7422−7430.
(42) Wang, X.; Margerum, D. W. *Inorg. Chem.* **1994**, *33*, 1050−1055.
(43) Liu, Q.; Margerum, D. W. *Environ. Sci. Technol.* **2001**, *35*, 1127−1133.
(44) Ershov, B. G.; Kelm, M.; Janata, E.; Gordeev, A. V.; Bohnert, E. *Radiochim. Acta* **2002**, *90*, 617−622.
(45) Ringeisen, B. R.; Muenter, A. H.; Nathanson, G. M. *J. Phys. Chem. B* **2002**, *106*, 4988−4998.
(46) Morris, J. R.; Behr, P.; Antman, M. D.; Ringeisen, B. R.; Splan, J.; Nathanson, G. M. *J. Phys. Chem. A* **2000**, *104*, 6738−6751.
(47) Ringeisen, B. R.; Muenter, A. H.; Nathanson, G. M. *J. Phys. Chem. B* **2002**, *106*, 4999−5010.
(48) Our inability to observe reaction of BrCl with glycerol is in accord with ref 16, which also could not detect reaction of BrCl with liquid water. The hydrolysis of Cl_2 and Br_2 is very slow (ref 42), although an analogous study (ref 43) for BrCl reports a rate of 10^6 s^{-1}.
(49) King, D. A.; Wells, M. G. *Surf. Sci.* **1972**, *2*, 454−482.
(50) Brastad, S. M.; Nathanson, G. M. *Phys. Chem. Chem. Phys.* **2011**, *13*, 8284−8295.
(51) In order to correct for differences in the Cl_2 beam fluxes in the pure and salty glycerol measurements, TOF spectra are recorded each time from the Teflon block hanging from the reservoir. These TOF spectra provide scaling factors to correct for day-to-day fluctuations and are found to be close to 1.
(52) Muenter, A. H.; DeZwaan, J. L.; Nathanson, G. M. *J. Phys. Chem. C* **2007**, *111*, 15043−15052.
(53) Danckwerts, P. V. *Gas−Liquid Reactions*; McGraw-Hill: New York, 1970.
(54) A lower limit to the diffusion-controlled reaction rate of 4×10^6 s^{-1} in 2.7 M NaBr−glycerol was obtained from rate = $4\pi\{D(Cl_2) + D(Br^-)\}R[Br^-]$, where R is the reaction distance. The diffusion coefficients $D(Cl_2) \approx 3 \times 10^{-9}$ cm^2 s^{-1} and $D(Br^-) \approx 4 \times 10^{-9}$ cm^2 s^{-1} were obtained from the ∼5000-fold higher viscosity of NaBr−glycerol than that of pure water. A lower limit to R of 3 Å is given in Figure 1 of ref 63.
(55) Worsnop, D. R.; Zahniser, M. S.; Kolb, C. E.; Gardner, J. A.; Watson, L. R.; Van Doren, J. M.; Jayne, J. T.; Davidovits, P. *J. Phys. Chem.* **1989**, *93*, 1159−1172.
(56) Jones, R. H.; Olander, D. R.; Siekhaus, W. J.; Schwarz, J. A. *J. Vac. Sci. Technol.* **1972**, *9*, 1429.
(57) Linke, W. F. *Solubilities: Inorganic and Metal-Organic Compounds*, 4th ed.; Van Nostrand: Princeton, NJ, 1958; Vol. *1*.
(58) The near-interfacial concentration of Cl^- from the absorption of Cl_2 may be estimated by assuming a Cl_2 beam flux J of 1×10^{15} cm^{-2} s^{-1} and uptake γ of 0.24 over an exposure time of $t_{exp} = 0.12$ s. The two Cl^- ions produced by reaction to Br_2 diffuse over a depth of roughly $(Dt_{exp})^{1/2}$ to give a concentration of $(2\gamma J t_{exp})/(Dt_{exp})^{1/2} \approx 0.005$ M Cl^- for $D = 3 \times 10^{-9}$ cm^2 s^{-1}.
(59) Reactions of Br^- and Cl^- have been measured for $Cl_2 + Br^-$ and $Cl_2 + Cl^-$, where $k(Br^-)/k(Cl^-) = 3 \times 10^5$, and BrCl + Br^- and BrCl + Cl^-, where $k(Br^-)/k(Cl^-) > 100$. See Table 1 of refs 43 and 44.
(60) The reaction $Br_2Cl^- \rightarrow Br_2 + Cl^-$ is considered to dominate over $Br_2Cl^- \rightarrow BrCl + Br^-$ based on the 20-fold ratio of rate constants for the analogous reactions $Cl_2Br^- \rightarrow Cl_2 + Br^-$ and $Cl_2Br^- \rightarrow BrCl + Cl^-$. See Table 1 of refs 43 and 44. Reference 69 also indicates that both reactions are endothermic in water, with values equal to + 27 and +50 kJ mol^{-1}, respectively.
(61) Bartlett, W. P.; Margerum, D. W. *Environ. Sci. Technol.* **1999**, *33*, 3410−3414.
(62) The reaction probability $\beta = \gamma^{Cl_2}$ of Cl_2 in 2.7 M NaBr−H_2O was extrapolated from measurements in Table 5 of ref 14 for a 0.5 M NaBr−H_2O solution at 293 K. γ^{Cl_2} equals $(1 - \gamma_s)\gamma_b + \gamma_s$, where γ_s and γ_b are uptake due to $Cl_2 + Br^-$ reaction at the surface and in the bulk. Each value was then scaled to 2.7 M NaBr according to their eqs 7 and 16, yielding $\gamma^{Cl_2} = 0.23$. The ratio of surface to bulk reaction probabilities is nearly 1 at 2.7 M NaBr.
(63) Rettner, C. T.; Auerbach, D. H. *Science* **1994**, *263*, 365−367.
(64) (a) Pathak, A. K.; Mukherjee, T.; Maity, D. K. *J. Phys. Chem. A* **2008**, *112*, 744. (b) An earlier study computed an interaction energy between Cl_2 and four water molecules of 11 kJ mol^{-1}, which is ∼1/3 as large as calculated by Pathak et al. See: Geiger, F. M.; Hicks, J. M.; de Dios, A. C. *J. Phys. Chem. A* **1998**, *102*, 1514.
(65) Lejonthun, L.; Andersson, P. U.; Nagard, M. B.; Pettersson, J. B. C. *J. Phys. Chem. B* **2006**, *110*, 23497−23501.
(66) We judge the 50 ps prediction to be a lower limit because Cl_2 rotational motion should be less impeded on the warm 291 K liquid than on the 125−135 K ice surface. This greater freedom of motion should lower the Arrhenius prefactor and therefore increase the residence time.
(67) Roeselová, M.; Jungwirth, P.; Tobias, D. J.; Gerber, R. B. *J. Phys. Chem. B* **2003**, *107*, 12690−12699.
(68) The estimate of 8×10^{13} cm^{-2} was obtained by counting the number of I^- ions in the 30 × 30 $Å^2$ area in Figure 9d in: Jungwirth, P.; Tobias, D. J. *J. Phys. Chem. B* **2002**, *106*, 6361.
(69) Ogawa, Y.; Takahashi, O.; Kikuchi, O. *THEOCHEM* **1998**, *429*, 187−196.
(70) Ault, B. S.; Andrews, L. *J. Chem. Phys.* **1976**, *64*, 4853−4859.
(71) Scott, R. L. *J. Am. Chem. Soc.* **1953**, *75*, 1550−1552.
(72) Popov, A. I. *Polyhalogen Complex Ions*; Academic Press: New York, 1967; Vol. *1*.
(73) Habold, R.; Jouanne, J.; Keller-Rudek, H.; Merlet, P.; Ohms-Bredemann, U.; Strametz, C.; Wagner, J.; Wietelmann, A. *Bromine; Gmelin Handbook of Inorganic and Organometallic Chemistry*; Springer-Verlag: Berlin, Germany, 1991; Vol. Supplement B3.
(74) King, D. L.; Herschbach, D. R. *Faraday Discuss. Chem. Soc.* **1973**, *55*, 331−343.
(75) Evans, J. C.; Lo, G. Y.-S. *J. Chem. Phys.* **1966**, *45*, 1069−1071.
(76) The diffusion coefficient D for Cl_2 in 2.7 M NaBr−glycerol was estimated to be 3×10^{-9} cm^2 s^{-1} using the water value of 1.5×10^{-5} cm^2 s^{-1} and the measured viscosity ratio of ∼5000. For the Cl_2 value in water, see: *CRC Handbook of Chemistry and Physics Online* 92nd ed.; CRC: Boca Raton, FL, 2011; section 6−249. The diffusion coefficients for BrCl, Br_2, Cl_2Br^-, and Br_2Cl^- were set equal to the Cl_2 value to simplify the numerical simulations. This assumption is likely to be correct to within a factor of two from a survey of ion diffusion coefficients in water.

(77) Joshipura, K. N.; Limbachiya, C. G. *Int. J. Mass Spectrom. Ion Processes* **2002**, *216*, 239−247.
(78) Carslaw, H. S.; Yaeger, J. C. *Conduction of Heat in Solids*; Oxford University Press: Oxford, U.K., 1959; p 53.
(79) Hanson, D. R.; Ravishankara, A. R. *J. Phys. Chem.* **1993**, *97*, 12309−12319.
(80) Shi, Q.; Li, Y. Q.; Davidovits, P.; Jayne, J. T.; Worsnop, D. R.; Mozurkewich, M.; Kolb, C. E. *J. Phys. Chem. B* **1999**, *103*, 2417−2430.
(81) Swartz, E.; Shi, Q.; Davidovits, P.; Jayne, J. T.; Worsnop, D. R.; Kolb, C. E. *J. Phys. Chem. A* **1999**, *103*, 8824−8833.
(82) Crank, J. *Mathematics of Diffusion*, 2nd ed.; Oxford University Press: London, 1975; pp 104−136.
(83) Danckwerts, P. V. *Trans. Faraday Soc.* **1951**, *47*, 1014.
(84) Shi, Q.; Davidovits, P.; Jayne, J. T.; Worsnop, D. W.; Kolb, C. E. *J. Phys. Chem. A* **1999**, *103*, 8812−8823.